International Journal of Power Electronics and Drive Systems (IJPEDS)
Vol. 12, No. 4, December 2021, pp. 2470~2482
ISSN: 2088-8694, DOI: 10.11591/ijpeds.v12.i4.pp2470-2482

Performance improvement of the variable speed wind turbine driving a DFIG using nonlinear control strategies

Chojaa Hamid[1], A. Derouich[2], T. Hallabi[3], O. Zamzoum[4], M. Taoussi[5], S. Rhaili[6], O. Boulkhrachef[7]
[1,2,4,5]Laboratory of Technologies and Industrial Services, Higher School of Technology, Sidi Mohamed Ben Abdellah University, Fez 30000, Morocco
[3]Engineering Research Laboratory LRI, Hassan II University, ENSEM, Casablanca, Morocco
[6]Department of Electrical Engineering, Mohammadia School of Engineers, Mohammed V University in Rabat, Morocco
[7]Laboratoire L2EI, University of Jijel, Jijel, Algeria

Article Info

Article history:

Received Mar 4, 2021
Revised Sep 6, 2021
Accepted Sep 15, 2021

Keywords:

Backstepping controller
DFIG
Field oriented control
MPPT strategy
Sliding mode approach
Wind energy

ABSTRACT

In this research paper, a nonlinear Backstepping controller has been proposed in order to improve the dynamic performance of a doubly fed induction generator (DFIG) based Wind Energy conversion System, connected to the grid through a back-to-back converter. Firstly, an overall modeling of proposed system has been presented. Thereafter, three control techniques namely backstepping (BSC), sliding mode (SMC) and field-oriented control (FOC) using a conventional PI regulator have been designed in order to control the stator active and reactive powers of the DFIG. In addition, the maximum power point tracking (MPPT) strategy has been investigated in this work with three mechanical speed controllers: BSC, SMC and PI controller with the aim of making a synthesis and a comparison between their performances to determine which of those three techniques is more efficient to extract the maximum power. Finally, a thorough comparison between the adopted techniques for the DFIG control has been established in terms of response time, rise time, total harmonic distortion (THD) (%) of the stator current, static errors and robustness. The effectiveness and robustness of each control approach has been implemented and tested under MATLAB/Simulink environment by using a 1.5 MW wind system model.

Corresponding Author:

Chojaa Hamid
Laboratory of Technologies and Industrial Services
Higher School of Technology, Sidi Mohamed Ben Abdellah University, Fez 30000, Morocco
Email: hamid.chojaa@usmba.ac.ma

NOMENCLATURE

β (Degree °)	: blade pitch angle	Pv (W)	: power of the wind turbine
λ	: tip speed ratio or Lambda	Ps(W), Qs (Var)	: active and reactive power
Cp	: Power coefficient	ϕs, ϕr (Wb)	: stator and rotor flux
ρ (Kg/m3)	: Air density	Vs, Vr (V)	: stator and rotor voltage
V (m/s)	: wind speed	is, ir (A)	: stator and rotor current
R (m)	: blade radius	ωs, ωr (rad/s)	: stator and rotor pulsations
S (m²)	: wind turbine blades swept area (= π*R²)	Ωg (rad/s)	: mechanical speed
Paer (W)	: aerodynamic power	RSC	: rotor side converter
Caer (N.m)	: aerodynamic torque	GSC	: grid side converter

1. INTRODUCTION

Many nations are looking to develop an alternative solution based on renewable energy sources, like solar and wind energy, that impacts the environment in a positive way and contributes to the CO_2 emissions reduction [1], [2]. Actually, the wind power source is categorized as one of the most efficient and robust technologies to achieve this objective. Moreover, to bypass the old sources and generate a cleaner energy, the variable speed wind turbines configuration has attracted many researches, due to the fact that it offers more dynamic and effectiveness than the fixed speed turbines through raising the energy quality, reducing the mechanical pressure and increasing the extracted power [3]. On the other side, the variable speed wind turbine (VSWT) that uses a synchronous generator, or permanent magnetic synchronous generator (PMSG), basically needs a full converter in the stator side [4]-[6]. However, in VSWTs that operates with a doubly fed induction generator (DFIG), only a partial converter is necessary in the rotor side [7]. That is to say that the DFIG based wind turbine is more adequate. Furthermore, it can attain high efficiency and maximize the extracted energy from the wind, which makes it an attractive option to be used for its several benefits and robustness [8], [9].

Various control techniques have been proposed in the literature to monitor the wind turbine during wind speed variations and external disturbances, and to achieve the highest rate of efficiency, such as filed oriented control (FOC) based on PI controller, however the performance can be demoted if the system internal gains are changed [10], [11]. To overcome the drawbacks of FOC, several advanced nonlinear approaches can be used to enhance WECS robustness. Referring to [12], an adaptive control has been implemented, and the robustness was high under abrupt speed changes. Nonetheless, various design parameters reveal when this approach is applied. Thus, they affect the controlled system performance.

Robust control design using Neuronal network algorithm has proposed in [13]. The Simulations show an efficient performance in term of overshoot and response time. Yet, this approach needs an abundant parameter adjusted and a massive data in the training phase. The authors in [14] designed a fuzzy logic controller in order to control WECS. The controller delivers an appropriate result with fluctuations in generator velocity due to the several tuning parameters of the mentioned algorithm. Sliding Mode Control (SMC) is a good solution to control the DFIG due to its robustness, but even so, a pure SMC suffers from the chattering effect. Amidst the limitations of above-mentioned technologies, nonlinear Backstepping control is proposed and tested on a high power DFIG based WECS in this study, for its many advantages in terms of performances improvement, simplicity of implementation, and robustness against the external disturbances [15], [16]. Moreover, the system stability can be ensured by applying Lyapunov function. In order to prove the effectiveness of the suggested control, a comparison has been conducted in this paper with an improved sliding mode approach using (sat) function as a replacement of the regular (sign) function to reduce the chattering problem. Moreover, an overall comparison of the collected results with other published works has been made regarding precision, efficacy, quality of injected power, set-point tracking, response time, static errors, and minimizing the total harmonic distortion (THD).

This paper is organized as follows: after the introduction that is bringing a general review in literature, section 2, came to present the modeling of the wind energy system, and the MPPT control strategy. Thereafter, section 3 deals with the implementation of vector control on the DFIG. Then, section 4 examines the proposed Sliding Mode Algorithm, while section 5 explains the suggested backstepping strategy of DFIG. Subsequently, section 6 introduces the modelling of the rotor side converter. Then, the simulation results are shown in section 7. Finally, section 8 summarizes the conclusion.

2. WIND ENERGY CONVERSION SYSTEM MODEL

DFIG based wind energy system is represented by the simplified schematic diagram of Figure 1. This electrical machine has a rotor circuit connected to the grid through back-to-back power electronic converters, while the stator circuit is directly connected to the power grid.

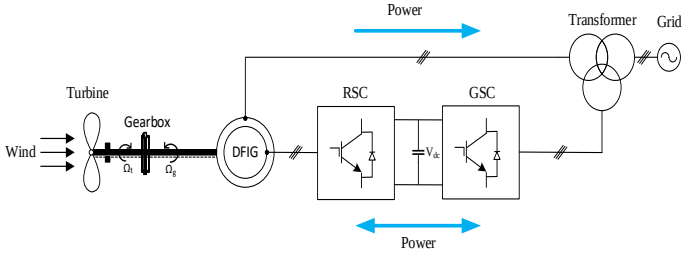

Figure 1. Wind energy conversion system configuration

2.1. Modeling of the wind turbine and MPPT control strategy

The mathematical model of the turbine is expressed by the following [17]:

$$P_V = \frac{\rho S V^3}{2} \tag{1}$$

$$P_{aer} = C_p P_V = \frac{1}{2}\rho\pi R^2 V^3 C_p(\lambda,\beta) \tag{2}$$

The aerodynamic power coefficient C_p as a function of the tip speed ratio (TSR) λ and the pitch angle β is giving by I. Yasmine and B. Badre [18]:

$$\begin{cases} Cp\,(\lambda,\beta) = 0.5\left(\frac{116}{\lambda i} - 0.4\beta - 5\right) exp\left(\frac{-21}{\lambda i}\right) + 0.0068\,\lambda \\ \frac{1}{\lambda i} = \frac{1}{\lambda+0.08\beta} - \frac{0.035}{\beta^3+1} \quad ; \quad \lambda = \frac{\Omega_t R}{V} \end{cases} \tag{3}$$

The variation of the power coefficient (C_p) as a function of (TSR) is illustrated in Figure 2. As it can be seen, the maximum value of Cpmax=0.479 is obtained when λopt=8.1 and β = 0.

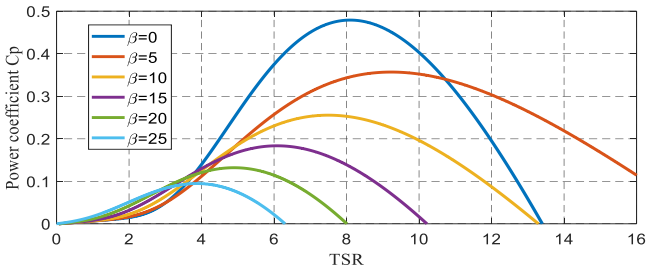

Figure 2. The power coefficient C_p curve versus the speed ratio TSR for several blade angles

The electromagnetic and mechanical torques equations are related by:

$$J\frac{d\Omega_g}{dt} = C_{mec} = C_g - C_{em} - C_f \tag{4}$$

where $J = \frac{J_t}{G^2} + J_g$, $C_f = f_v\Omega_g$. f_v coefficient of fractionate. J_t, J_g and J inertia of the turbine, generator and the total inertia. C_g, C_{em}, C_f are the torque applied on the generator, the electromagnetic torque and the torque resulting from the viscous friction, respectively.

To capture the maximum of the wind energy, the rotational speed of the turbine must be continuously adjusted according to the wind speed variations [19]. The main goal of this command is to adjust continuously the turbine rotational speed at the value that guarantees an optimal speed ratio (λopt).

In this paper, The MPPT technique has been realized with mechanical speed control as shown in Figure 3. This control strategy consists of adjusting the electromagnetic torque that is developed by the electrical generator in order to fix it at its reference value. To achieve this, a speed control has been used to ensure that the mechanical speed is equal to the reference speed. This speed regulation has been processed by three types of controllers with a view to make a synthesis and a comparison between those three controllers.

2.3.1.PI controller

The closed-loop transfer function can be written as:

$$\frac{\Omega_{g(s)}}{\Omega_{g^*(s)}} = \frac{2\xi.\omega_n.s+\omega_n^2}{s^2+2\xi.\omega_n.s+\omega_n^2} = \frac{\frac{K_i+K_p.S}{J}}{s^2+\frac{Kp.fv}{J}.s+\frac{K_i}{J}} \tag{5}$$

The parameters K_p and K_i of the PI controller are given by:

$$\begin{cases} K_p = 2\xi.\omega_n.J - f_V \\ K_i = J.\omega_n^2 \end{cases} \tag{6}$$

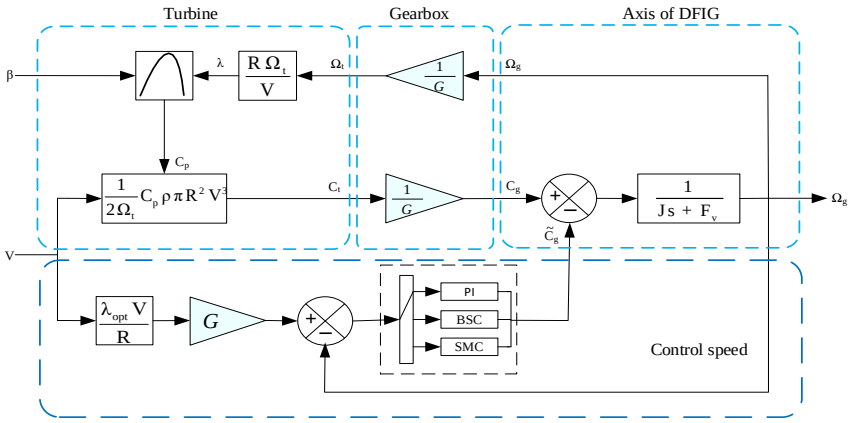

Figure 3. Block diagram of the maximum power point tracking technique using speed control

2.3.2.Backstepping controller

To design a backstepping control of the mechanical speed. We start by defining the tracking error of the set point as [20]:

$$e(\Omega_g) = \Omega_g^* - \Omega_g \tag{7}$$

We consider the following Lyapunov function:

$$v(e) = \frac{1}{2} e(\Omega_g)^2 \tag{8}$$

By deriving (9) and using the speed dynamic in (4), The Lyapunov function derivative can be formulated as:

$$\dot{v}(e) = e(\Omega_g).\dot{e}(\Omega_g) = e(\Omega_g).\left(\dot{\Omega}_g^* + \frac{1}{J}(C_{em} + f_v.\Omega_g - C_g)\right) \tag{9}$$

The stabilizing control of backstepping is defined as follows:

$$C_{em}^* = -J.\dot{\Omega}_g^* - f_v.\Omega_g + C_g - K_1.e(\Omega_g) \tag{10}$$

With K_1 is a positive constant. By substituting the (10) in (9), the result can be given as:

$$\dot{v}(e) = -K_1.e(\Omega_g)^2 < 0 \tag{11}$$

2.3.3.Sliding mode controller

To determine the command magnitude C_{em}^*, the relative degree of the surface is equal to one. The sliding surface is defined by:

$$S(\Omega_g) = \Omega_g^* - \Omega_g \tag{12}$$

We consider the following Lyapunov function:

$$V\left(S(\Omega_g)\right) = \frac{1}{2} S(\Omega_g)^2 \tag{13}$$

The Lyapunov function derivative can be expressed as:

$$\dot{V}\left(S(\Omega_g)\right) = S(\Omega_g).\dot{S}(\Omega_g) \tag{14}$$

With $\dot{S}(\Omega_g) = \dot{\Omega}_g^* - \dot{\Omega}_g$ (15)

By replacing the (4), We get:

$$\dot{S}(\Omega_g) = \dot{\Omega_g^*} + \frac{1}{J}(C_{em} + f_v.\Omega_g - C_g) \quad (16)$$

Replacing the command C_{em} by its equivalent components $(C_{emeq} + C_{emn})$ in (16), we find:

$$\dot{S}(\Omega_g) = \dot{\Omega_g^*} + \frac{1}{J}\left((C_{emeq} + C_{emn}) + f_v.\Omega_g - C_g\right) \quad (17)$$

During the sliding mode and in the steady state we have: $S(\Omega_g) = 0$; $\dot{S}(\Omega_g) = 0$ and $C_{emn} = 0$. From these statements, we can extract the expression of the equivalent command C_{emeq} as the following:

$$C_{emeq} = -J.\dot{\Omega_g^*} - f_v.\Omega_g + C_g \quad (18)$$

Replacing the (18) in (17), the result became as:

$$\dot{S}(\Omega_g) = \frac{1}{J}C_{emn} \quad (19)$$

To ensure the convergence of Lyapunov's function, we set:

$$C_{emn} = -K_2.\text{sign}\left(S(\Omega_g)\right) \quad (20)$$

Such as $K_2$is a positive constant.

2.2. Modeling of the wind turbine and MPPT control strategy

The general mathematical equations of the voltages, flux and active/reactive powers of the doubly fed induction generator in the dq Park reference are given by the following expressions [21], [22]:

voltage equations :

$$\begin{cases} V_{sd} = R_s i_{sd} + \frac{d}{dt}\phi_{sd} - \omega_s \phi_{sq} \\ V_{sq} = R_s i_{sq} + \frac{d}{dt}\phi_{sq} + \omega_s \phi_{sd} \\ V_{rd} = R_r i_{rd} + \frac{d}{dt}\phi_{rd} - (\omega_s - \omega_r)\phi_{rq} \\ V_{rq} = R_r i_{rq} + \frac{d}{dt}\phi_{rq} + (\omega_s - \omega_r)\phi_{rd} \end{cases} \quad (21)$$

flux equations :

$$\begin{cases} \phi_{sd} = L_s i_{sd} + L_m i_{rd} \\ \phi_{sq} = L_s i_{sq} + L_m i_{rq} \\ \phi_{rd} = L_r i_{rd} + L_m i_{sd} \\ \phi_{sq} = L_r i_{rq} + L_m i_{sq} \end{cases} \quad (22)$$

power equations :

$$\begin{cases} P_s = \frac{3}{2} Re\{\vec{V_s} \times \vec{I_s^*}\} = \frac{3}{2}(V_{sd} i_{sd} + V_{sq} i_{sq}) \\ Q_s = \frac{3}{2} Im\{\vec{V_s} \times \vec{I_s^*}\} = \frac{3}{2}(V_{sq} i_{sd} - V_{sd} i_{sq}) \end{cases} \quad (23)$$

where ω_s is the pulsation of the stator variables and ω_r is the pulsation of the rotor ones. This last parameter is given by:

$$\omega_r = \omega_s - p.\Omega_g \quad (24)$$

The electromagnetic torque is expressed as:

$$C_{em} = \frac{3}{2} p \frac{L_m}{L_s} Im\{\overrightarrow{\Psi_s} \times \overrightarrow{I_r^*}\} = \frac{3}{2} p \frac{L_m}{L_s}(\phi_{sq} i_{rd} - \phi_{sd} i_{rq}) \quad (25)$$

3. APPLICATION OF THE VECTOR CONTROL ON THE DFIG

The asynchronous machine can adopt several types of control such as vector control, which ensures decoupling between its variables and makes it similar to a DC generator [23]-[25]. To decouple the control of active and reactive power, we adopt in this work the technique of stator field orientation. By setting the stator field vector aligned with d-axis, we obtain:

$$\begin{cases} \emptyset_{sq} = 0 \\ \emptyset_{sd} = \Psi_s \end{cases} \tag{26}$$

$$\begin{cases} V_{sq} = 0 \\ V_{sd} = V_s = \omega_s \Psi_s \end{cases} \tag{27}$$

According to this statement, the (22) can be simplified:

$$\begin{cases} i_{sd} = \frac{\Psi_s}{L_s} - \frac{L_m}{L_s} i_{rd} \\ i_{sq} = -\frac{L_m}{L_s} i_{rq} \end{cases} \tag{28}$$

The expression of the rotor flux becomes:

$$\begin{cases} \emptyset_{rd} = \sigma L_r i_{rd} + \frac{L_m}{L_s} \Psi_s \\ \emptyset_{rq} = \sigma L_r i_{rq} \end{cases} \tag{29}$$

With $\sigma = 1 - \frac{L_m^2}{L_s L_r}$ is the dispersion coefficient of Blondel.

From (21), we deduce the expressions of the control variables V_{rd} and V_{rq}:

$$\begin{cases} V_{rd} = R_r i_{rd} + \sigma L_r \frac{d}{dt} i_{rd} - g\omega_s \sigma L_r i_{rq} \\ V_{rq} = R_r i_{rq} + \sigma L_r \frac{d}{dt} i_{rq} + g\omega_s \sigma L_r i_{rd} + g\frac{L_m V_s}{L_s} \end{cases} \tag{30}$$

Replacing the expressions of i_{sd}, i_{sq} and $\emptyset_{sd}$ in the expression of the electromagnetic torque and the stator active and reactive powers in (23) and (25), we can express C_{em}, P_s and Q_s by (31) and (32) respectively:

$$C_{em} = -\frac{3}{2} p \frac{L_m}{L_s} \Psi_s i_{rq} = -\frac{3}{2} p \frac{L_m V_s}{L_s \omega_s} i_{rq} \tag{31}$$

$$\begin{cases} P_s = -\frac{3}{2} V_s \frac{L_m}{L_s} i_{rq} \\ Q_s = \frac{3}{2}\left(V_s \frac{\Psi_s}{L_s} - V_s \frac{L_m}{L_s} i_{rd}\right) \end{cases} \tag{32}$$

4. APPLICATION OF THE SLIDING MODE CONTROL OF DFIG

The sliding mode knew a big success during last years. It is due to its implementation simplicity and the robustness with regard to the system uncertainties and the external disturbances. The SMC consists to return the state trajectory towards the sliding surface and to develop it above, with a certain dynamic up to the equilibrium [26]. The sliding mode control goes through three stages:

- Choice the switching surface
- Convergence condition
- Calculation of the control laws

The stator active and reactive powers control surfaces have the form:

$$\begin{cases} S(P_s) = P_s^{ref} - P_s \\ S(Q_s) = Q_s^{ref} - Q_s \end{cases} \tag{33}$$

The derivatives of the surfaces are obtained as:

$$\begin{cases} \dot{S}(P_s) = (\dot{P}_s^{ref} - \dot{P}_s) \\ \dot{S}(Q_s) = (\dot{Q}_s^{ref} - \dot{Q}_s) \end{cases} \quad (34)$$

We replace the expressions of active and reactive powers (32) in the last one:

$$\begin{cases} \dot{S}(P_s) = \left(\dot{P}_s^{ref} + \frac{3}{2}.V_s.\frac{L_m}{L_s}.\dot{I}_{rq}\right) \\ \dot{S}(Q_s) = \dot{Q}_s^{ref} - (-\frac{3}{2}.V_s.\frac{Lm}{L_s}.\dot{I}_{dr}) \end{cases} \quad (35)$$

The next step is to draw the expressions of the currents derivatives $\dot{I}_{rdq}$ from (30) and substitute it in the (36):

$$\begin{cases} \dot{S}(P_s) = \dot{P}_s^{ref} + \frac{3}{2}.V_s.\frac{Lm}{L_s.L_r.\sigma}\left(V_{rq} - R_r.i_{rq} \quad - g.\omega_s.\sigma.L_r.i_{rd} + g.\frac{L_m.V_s}{\omega_s.L_s}\right) \\ \dot{S}(Q_s) = (\dot{Q}_s^{ref} + \frac{3}{2}.V_s.\frac{Lm}{L_s.L_r.\sigma}.\left(V_{dr} - R_r i_{rd} + g.\omega_s.\sigma.L_r.i_{rq}\right) \end{cases} \quad (36)$$

Replacing V_{rdq} by $\left(V_{rdq}^{eq} + V_{rdq}^{n}\right)$, the controls principals appears clearly in (37):

$$\begin{cases} \dot{S}(P_s) = \dot{P}_s^{ref} + \frac{3}{2}.V_s.\frac{Lm}{L_s.L_r.\sigma}.((V_{rq}^{eq} + V_{rq}^{n}) - R_r.i_{rq} - g.\omega_s.\sigma.L_r.i_{rd} + g.\frac{L_m.V_s}{\omega_s.L_s}) \\ \dot{S}(Q_s) = (\dot{Q}_s^{ref} + \frac{3}{2}.V_s.\frac{Lm}{L_s.L_r.\sigma}.((V_{rd}^{eq} + V_{rd}^{n}) - R_r i_{rd} + g.\omega_s.\sigma.L_r.i_{rq}) \end{cases} \quad (37)$$

During the sliding mode and in the steady state, we have:

$$\begin{cases} S(P_s) = 0, \quad \dot{S}(P_s) = 0, \quad V_{rq}^{n} = 0 \\ S(Q_s) = 0, \quad \dot{S}(Q_s) = 0, \quad V_{rd}^{n} = 0 \end{cases} \quad (38)$$

The equivalents control components V_{rdq}^{eq} can deduced as:

$$\begin{cases} V_{rq}^{eq} = -\frac{2}{3}.\frac{\sigma.L_s.L_r}{V_s.Lm}.\dot{P}_s^{ref} + R_r.i_{rq} + g.\omega_s.\sigma.L_r.i_{rd} - g.\frac{L_m.V_s}{\omega_s.L_s} \\ V_{rd}^{eq} = -\frac{2}{3}.\frac{\sigma.L_s.L_r}{V_s.M}.\dot{Q}_s^{ref} + R_r i_{rd} - g.\omega_s.\sigma.L_r.i_{rq} \end{cases} \quad (39)$$

During the convergence mode, so that the conditions $S(P).\dot{S}(P) \leq 0$ and $S(Q).\dot{S}(Q) \leq 0$ are satisfied, we assume:

$$\begin{cases} \dot{S}(P_s) = \frac{3}{2}.V_s.\frac{Lm}{L_s.L_r.\sigma}.V_{rq}^{n} \\ \dot{S}(Q_s) = \frac{3}{2}.V_s.\frac{Lm}{L_s.L_r.\sigma}.V_{rd}^{n} \end{cases} \quad (40)$$

Therefore, the switching terms given by:

$$\begin{cases} V_{rq}^{n} = -K_{Vq}.(S(P_s)) \\ V_{rd}^{n} = -K_{Vd}.(S(Q_s)) \end{cases} \quad (41)$$

To check the stability condition of the system, the parameters K_{Vd} and K_{Vq} must be positive. In order to reduce any possible overshooting of the voltages components V_{rdq}, it is often useful to add voltages limiters, which expressed by:

$$\begin{cases} V_{rq}^{lim} = V_{rq}^{max}.sat(P_s) \\ V_{rd}^{lim} = V_{rd}^{max}.sat(Q_s) \end{cases} \quad (42)$$

5. BACKSTEPPING CONTR OL OF THE DFIG

The backstepping approach is a recursive technique design for stabilizing highly nonlinear dynamical system [27]. The principle of the backstepping controller is the use of a virtual control to decompose a complex nonlinear system problem into various simpler design steps. The stability and performance of the system is achieved by using a Lyapunov function that is used to drive the virtual control [28], [29]. The errors between the reference and the measured signals of stator active and reactive powers are defined as [30].

$$\begin{cases} e_1 = P_s^{ref} - P_s \\ e_2 = Q_s^{ref} - Q_s \end{cases} \tag{43}$$

Their derivates are given as:

$$\begin{cases} \dot{e}_1 = \dot{P}_s^{ref} + \frac{V_s.Lm}{\sigma.L_r.L_s}\left(V_{rq} - R_r.i_{rq} - \sigma.L_r.\omega_r.i_{rd} + g.\frac{L_m.V_s}{\omega_s.L_s}\right) \\ \dot{e}_2 = \dot{Q}_s^{ref} + \frac{V_s.Lm}{\sigma.L_r.L_s}\left(V_{rd} - R_r.i_{rd} + \sigma.L_r.\omega_r.i_{rq}\right) \end{cases} \tag{44}$$

The choosed Lyapunov function is formulated as:

$$\begin{cases} V_{(e_1)} = \frac{1}{2}e_1^2 \\ V_{(e_1,e_2)} = \frac{1}{2}e_1^2 + \frac{1}{2}e_2^2 \end{cases} \tag{45}$$

The derivative of each error Lyapunov function is written as follow:

$$\begin{cases} \dot{V}_{(e_1)} = e_1.\dot{e}_1 = e_1.\left(\dot{P}_s^{ref} + \frac{V_s.Lm}{\sigma.L_r.L_s}\left(V_{rq} - R_r.i_{rq} - \sigma.L_r.\omega_r.i_{rd} + g.\frac{L_m.V_s}{\omega_s.L_s}\right)\right) \\ \dot{V}_{(e_2)} = e_1.\dot{e}_1 + e_2.\dot{e}_2 = -K_1.e_1^2 + e_2\left(\dot{Q}_s^{ref} + \frac{V_s.Lm}{\sigma.L_r.L_s}\left(V_{rd} - R_r.i_{rd} + \sigma L_r.\omega_r.i_{rq}\right)\right) \end{cases} \tag{46}$$

The control voltages selected as follows:

$$\begin{cases} V_{rq}^{ref} = -\frac{\sigma.L_s.L_r}{V_s.L_m}.\dot{P}_s^{ref} + R_r i_{rd} + \omega_r.\sigma.L_r.i_{rd} - g.\frac{L_m.V_s}{\omega_s.L_s} - \frac{\sigma.L_s.L_r}{V_s.Lm}.K_3.e_1 \\ V_{rd}^{ref} = -\frac{\sigma.L_s.L_r}{V_s.L_m}.\dot{Q}_s^{ref} + R_r i_{rd} - \omega_r.\sigma.L_r.i_{rq} - \frac{\sigma.L_s.L_r}{V_s.Lm}.K_4.e_2 \end{cases} \tag{47}$$

Where: K_3 and K_4 are positives constants.

6. GRID SIDE CONVERTER

The d-q axis components of the grid side converter are formulated as:

$$\begin{cases} V_{fd} = R_f.i_{fd} + L_f.\frac{di_{fd}}{dt} - w_s.L_f.i_{fq} \\ V_{fq} = R_f.i_{fq} + L_f.\frac{di_{fq}}{dt} + w_s.L_f.i_{fd}.V_{gq} \end{cases} \tag{48}$$

the voltage of the DC link [21].

$$\begin{cases} i_{gm} = \frac{P_r - P_c}{U_{dc}} = C\frac{dU_{dc}}{dt} \\ P_c = U_{dc}.i_c \\ P_r = U_{dc}.i_{rm} \end{cases} \tag{49}$$

where i_{rm} and i_{gm} represents the outputs currents of rotor side converter and grid side converter, respectively. The active and reactive power expressed as:

$$\begin{cases} P_g = V_{gq}.i_{fq} \\ Q_g = V_{gq}.i_{fd} \end{cases} \quad (50)$$

To illustrate the schematic diagram of the global control strategy for DFIG, a block diagram of the whole system is proposed in Figure 4.

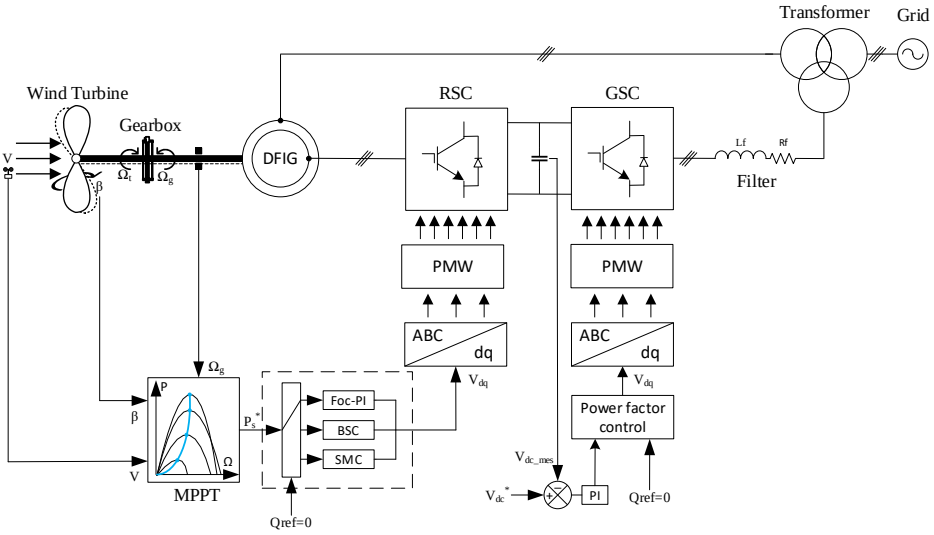

Figure 4. Schematic diagram of the global control strategy for DFIG

7. SIMULATION RESULTS AND DISCUSSION

In order to evaluate the performance of the wind energy conversion chain, equipped with the MPPT control strategy with mechanical speed control and two power converters connected to the rotor and to the grid (RSC and GSC) as shown in Figure 1. We performed a series of simulations in the MATLAB/Simulink environment, under an instantaneous wind speed profile, varying between 8m/s and 12m/s as Figure 5 (a) demonstrates. The studied global system parameters are listed in Table 1.

Table 1. Parameters of MATLAB/Simulink

Parameters of turbine, DC BUS and RL filter	Value	Parameters of DFIG	Value
Number of blades	3	Rated power, Pn	1.5 MW
Blade radius R	35.25 m	Stator rated voltage, Vs	698 V
Gearbox gain G	90	Stator rated frequency, f	50 Hz
Friction coefficient f	0.0024 N.m.s/rad	Stator resistance, Rs	0.012 Ω
Moment of inertia J	1000Kg.m²	Rotor resistance, Rr	0.021 Ω
DC-link capacitor C	8*10-3 F	Stator inductance, Ls	0.0137 H
filter inductance L_f	0.005 H	Rotor Inductance, Lr	0.0136 H
filter resistance R_f	0.012 Ω	Mutual inductance, M	0.0135 H
DC-link voltage U_{dc}	1200 V	Number of pair of poles, p	2

The functioning of the wind energy system tested and simulated by three types of control: direct vector control based on the PI controller, sliding mode control and Backstepping control. The purpose of this test is to make a comparison between the different control strategies developed and synthesized on the wind energy system. This comparison carried out from a series of tests performed during transient and permanent functioning of the system in terms of response time, static error, precision, reference point tracking, and the THD harmonic distortion rate of the stator currents.

The functioning of the wind energy system has been tested and simulated using three types of control: direct vector control based on the PI controller, sliding mode control and Backstepping control. The purpose of this test is to make a comparison between the different developed and synthesized control strategies on the wind energy system. This comparison is carried out after a set of tests that has been performed during transient and permanent functioning of the system in terms of response time, static error, precision, reference point tracking, and the THD harmonic distortion rate of the stator currents.

For the power coefficient Cp in Figure 5 (b), it takes a maximum value of 0.4799 with a pitch angle β= 0° for the three mechanical speed control strategies studied at the MPPT level: PI, sliding mode and the Backstepping method. However, it can be noted that the reference point tracking is followed in an identical way, in steady state, with a significant response time at start-up and slight fluctuations obtained by the control strategy based on the PI controller. On the other hand, the system responses show a slight overshoot for the relative speed λ in Figure 5 (c) and the mechanical speed in Figure 5 (d)) at start-up for the PI controller control. Whereas for the other two strategies the system follows the set point without any overshoot. Figure 5 (e) and Figure 5 (f) show satisfactory responses of the direct ird and quadratic irq components of the rotor current for the three control strategies: FOC-PI, SMC and BSC. These ird and irq currents have the same curves as the active power Ps in Figure 6 (a) and reactive power Qs in Figure 6 (b) respectively, reflecting the DFIG mathematical model. Thus, the active power controlled by the quadratic component of the current, while the reactive power controlled by the direct component of the current.

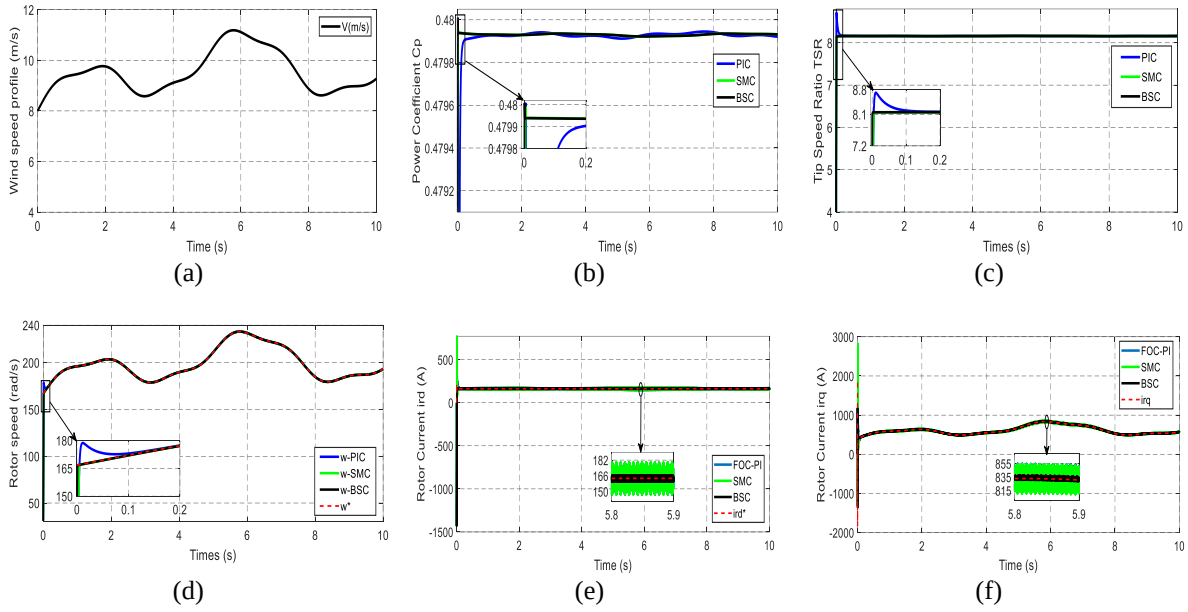

Figure 5. (a) wind speed (m/s), (b) power coefficient Cp (λ, β), (c) tip speed ratio TSR, (d) mechanical speed of the DFIG, (e) rotor current Ird, (f) rotor current Irq

In the most practical case, the machine coupled directly to the grid by the stator and driven by the rotor sizes through two bidirectional converters, and driven by a turbine. The stator active power Ps, depicted in Figure 6 (a), follows its reference generated by the MPPT technique and has the same variations as the applied wind speed profile, while the stator reactive power Qs in Figure 6 (b) is kept zero to keep the unit power factor and thus to optimize the quality of the generated electrical energy. The simulation results show that for all three-control strategies, the performance is similar. However, some differences can be identified. The response times of the active and reactive power as well as the oscillations are greater for the direct vector control technique based on the PI controller (FOC-PI) and for the sliding mode control technique (SMC). On the other hand, for the non-linear Backstepping method (BSC), there is no significant overshoot and a rapid convergence towards its reference value (lower response time).

Figure 6 (c) shows the electromagnetic torque Cem and its reference Cem* calculated using the MPPT control strategy to allow the wind turbine to operate under optimal conditions (MPPT). The tracking of the setpoint always ensured regardless of the reference variation and with different response time, overshoot and oscillations for the three control strategies. Note that the best values of the latter performance parameter are the values obtained when applying control by the backstepping technique. Figure 6 (d) shows the simulation result of the DC bus voltage. It is clear that its curve follows the reference with a fast transient response and low oscillations for the three control strategies applied. To ensure unity power factor at the stator side, we maintained the stator reactive power reference at zero (Qs* = 0VAR). To optimize the quality of the energy injected in the grid, the reactive power reference should allow keeping this factor optimal as shown in Figure 6 (e). Based on findings from the simulation, the unity power factor (cos ϕ = 1) is perfectly achieved by the reactive power control for the three control techniques in variable speed operation. However,

some low differences appear as in the response time, the precision and the static error with better values of the latter parameter obtained when applying the backstepping strategy.

Figures 6 (f), 7 (a) and 7 (b) illustrates the stator currents Is for the three phases. The currents injected into the electrical grid are sinusoidal with fs = 50 (Hz) for the three control strategies, despite the wind profile variations. The fast Fourier transformation is often common in the processing of signals. It transforms the signal in the frequency domain from its original domain (time domain). The Figures 7 (c)-(e) represent the analysis of the harmonic spectra for the phase "a" of the stator current Isa injected respectively for the three control strategies FOC-PI, SMC, and BSC. The BSC (THD=0.25%) offers a significant reduction in THD when compared to the SMC (THD=1.39%) ant the FOC used PI (THD=1.45%).

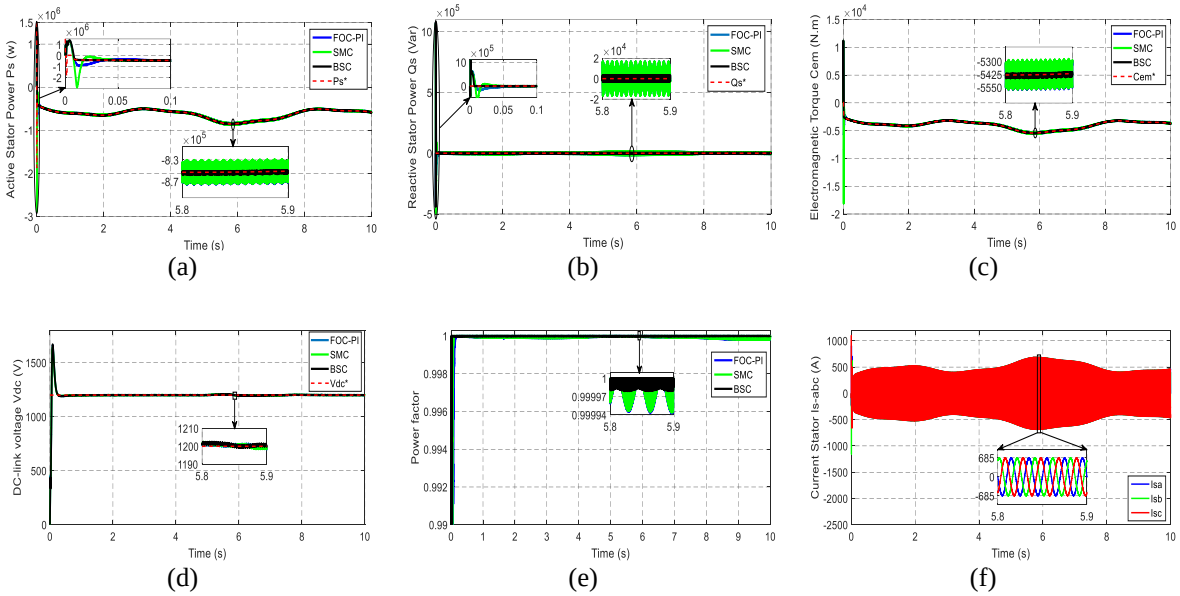

Figure 6. (a) active stator power Ps (W), (b) reactive stator power Qs (VAR), (c) electromagnetic torque tem (N.m) (d) DC-bus voltage, (e) stator current Is-abc (A) by the FOC-PI, (f) rotor Current Irq

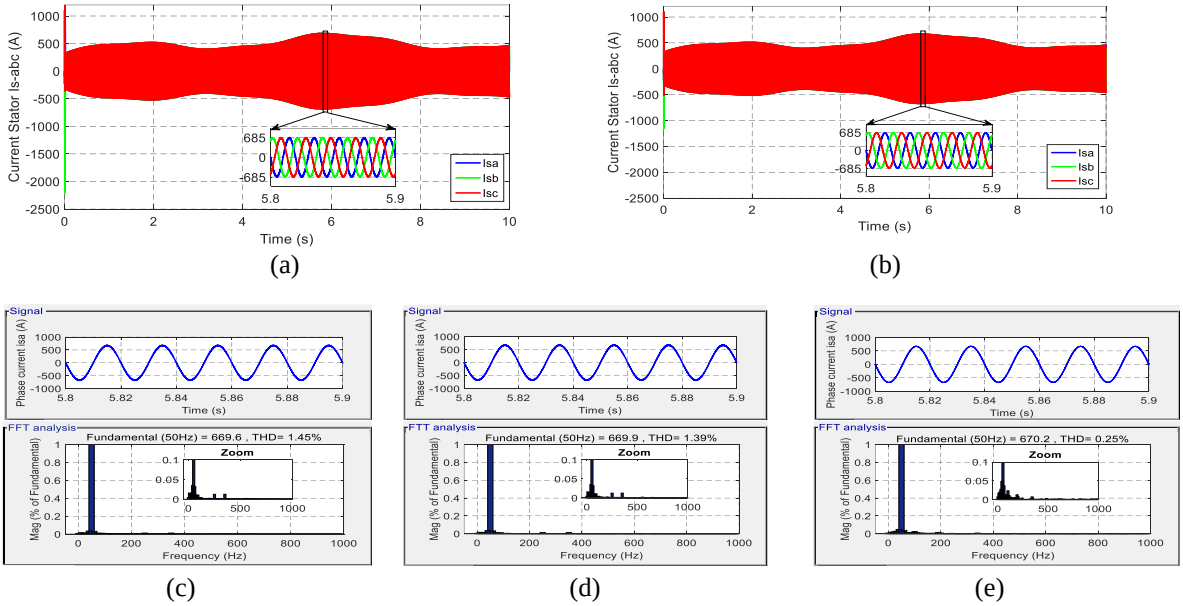

Figure 7. (a) stator current Is-abc (A) by the SMC, (b) stator current Is-abc (A) by the BSC, (c) spectrum analysis for the current injected isa by the FOC-PI, (d) spectrum analysis for the current injected Isa by the SMC, (e) spectrum analysis for the current injected Isa by the BSC *(continue)*

The Table 2. represents a synthesis of the comparison between the FOC with PI controllers, the SMC, and the BSC in terms of the response time, static error, set point tracking, precision, and THD (%) of the phase current 'is'. This Table 2 shows remarkable improvements obtained by BSC. These improvements include an optimization of the response time and the minimization in the harmonics in the stator current signals.

Table 2. Comparative synthesis between the foc using pi controllers, The SMC, and the BSC

Performance	FOC used PI	SMC	BSC
Response time (s)	0.408	0.295	0.175
Rise time (s)	0.226	0.163	0.097
Static errors (%)	0.24	0.19	0.11
Set-point tracking	Good	Very good	Very good
Precision	Medium	High	Very high
THD (%) of the current i_{sa}	1.45	1.39	0.25

8. CONCLUSION

This paper describes a comparative study between three different control techniques: backstepping (BSC), sliding mode (SMC) and Field oriented control (FOC) used conventional PI applied to the rotor side converter (RSC) of the wind energy conversion system (WECS) based on the DFIG. The MPPT technique with mechanical speed control using three controllers: BSC, SMC and PI controller also presented so that to keep the power coefficient of the system at its maximum value, thus the maximum wind power can be extracted. After testing and modeling the 1.5 MW wind system using MATLAB/Simulink software, the simulation results show that despite the robustness of the sliding mode control, it is clear that the latter presents the main problem of the chattering phenomenon that generates the harmonics and contribute to the mechanical part stress. In contrast, the application of backstepping has shown high performance and has proven to be the most suitable for the type of wind system chosen in comparison with to the two other control techniques studied in this work. Following this study, some suggestions and perspectives can made in order to be able to contribute, if possible, to the improvement of the functioning of the considered system: The possible integration of a storage system and the technical and economic optimization of the conversion chain, study of disturbances in the wind energy production with respect to network unbalance, voltage dips and fluctuations.

REFERENCES

[1] B. Beltran, T. Ahmed-Ali and M. E. H. Benbouzid, "Sliding Mode Power Control of Variable-Speed Wind Energy Conversion Systems," in *IEEE Transactions on Energy Conversion*, vol. 23, no. 2, pp. 551-558, June 2008, doi: 10.1109/TEC.2007.914163.

[2] M. El Azzaoui, H. Mahmoudi, "Modeling and control of a doubly fed induction generator base wind turbine system optimization of the power," *J. Theor. Appl. Inf. Technol.*, vol. 80, no. 2, October 2015.

[3] S. E. Rhaili, A. Abbou, S. Marhraoui, R. Moutchou, N. El Hichami, "Robust Sliding Mode Control with Five Sliding Surfaces of Five-Phase PMSG Based Variable Speed Wind Energy Conversion System," *International Journal of Intelligent Engineering and Systems*, vol. 13, no. 4, pp. 346-357, 2020, doi: 10.22266/ijies2020.0831.30.

[4] M. Alizadeh and S. S. Kojori Augmenting effectiveness of control loops of a PMSG (permanent magnet synchronous generator) based wind energy conversion system by a virtually adaptive PI (proportional integral) controller," *Energy*, vol. 91, pp. 610-629, November 2015, doi: 10.1016/j.energy.2015.08.047.

[5] S. Ganjefar and A. A. Ghasemi, "A novel-strategy controller design for maximum power extraction in stand-alone windmill systems," *Energy*, vol. 76(C), pp. 326-335, 2014, doi: 10.1016/j.energy.2014.08.024.

[6] S. M. Barakati, M. Kazerani and J. D. Aplevich, "Maximum Power Tracking Control for a Wind Turbine System Including a Matrix Converter," in *IEEE Transactions on Energy Conversion*, vol. 24, no. 3, pp. 705-713, Sept. 2009, doi: 10.1109/TEC.2008.2005316.

[7] D. Xie, Z. Xu, L. Yang, J. Østergaard, Y. Xue and K. P. Wong, "A Comprehensive LVRT Control Strategy for DFIG Wind Turbines With Enhanced Reactive Power Support," in *IEEE Transactions on Power Systems*, vol. 28, no. 3, pp. 3302-3310, Aug. 2013, doi: 10.1109/TPWRS.2013.2240707.

[8] M. Asghar, N. Ullah, "Performance comparison of wind turbine based doubly fed induction generator system using fault tolerant fractional and integer order controllers," in *Renew. Energy*, vol. 244-264, 2018, doi: 10.1016/j.renene.2017.01.008 116.

[9] S. Mensou, A. Essadki, T. Nasser, B. B. Idrissi, L. Ben Tarla, "Dspace DS1104 implementation of a robust nonlinear controller applied for DFIG driven by wind turbine," in *Renewable Energy*, vol. 147, pp. 1759-1771, Mar. 2020, doi: 10.1016/j.renene.2019.09.042.

[10] S. Mensou, A. Essadki, T. Nasser, B. B. Idrissi, "An efficient nonlinear backstepping controller approach of a wind power generation system based on a DFIG," in *Int. J. Renew. Energy Resour.*, vol. 7, no. 4, December 2017, pp. 1520-1528.

[11] M. Nadour, A. Essadki, and T. Nasser, "Comparative analysis between PI & backstepping control strategies of DFIG driven by wind turbine," in *Int. J. Renew. Energy Resour.*, vol. 7, no. 3, pp. 1307-1316September, 2017.
[12] F. Fateh, W. N. White and D. Gruenbacher, "A Maximum Power Tracking Technique for Grid-Connected DFIG-Based Wind Turbines," in *IEEE Journal of Emerging and Selected Topics in Power Electronics*, vol. 3, no. 4, pp. 957-966, Dec. 2015, doi: 10.1109/JESTPE.2015.2448633.
[13] K. Bedoud, M. Ali-Rachedi, T. Bahi, R. Lakel, and A. Grid, "Robust control of doubly fed induction generator for wind turbine under sub-synchronous operation mode," in *Energy Procedia*, vol. 74, pp. 886-899, 2015, doi: 10.1016/j.egypro.2015.07.824.
[14] A. Dida and D. Benattous, "A complete modeling and simulation of DFIG based wind turbine system using fuzzy logic control," in *Front. Energy*, vol. 10, pp. 143-154, 2016.
[15] T. Bakka, H. R. Karimi, and S. Christiansen, "Linear parameter-varying modelling and control of an offshore wind turbine with constrained information," in *IET Control Theory & Appl.*, vol. 8, no. 1, 2014, pp. 22-29, doi: 10.1049/iet-cta.2013.0480.
[16] Y. Ihedrane, C. El Bekkali, B. Bossoufi, M. Bouderbala, "Control of power of a DFIG generator with MPPT technique for wind turbines variable speed," in *Modeling, Identification and Control Methods in Renewable Energy Systems*, 2019, pp. 105-129, doi: 10.1007/978-981-13-1945-7_5.
[17] H. Chojaa, A. Derouich, S. E. Chehaidia, O. Zamzoum, M. Taoussi, and H. Elouatouat, "Integral sliding mode control for DFIG based WECS with MPPT based on artificial neural network under a real wind profile," in *Energy Reports*, vol. 7, pp. 4809-4824, 2021, doi: 10.1016/j.egyr.2021.07.066.
[18] I. Yasmine and B. Badre, "Improved Performance of DFIG-generators for Wind Turbines Variable-speed," in *International Journal of Power Electronics and Drive Systems*, vol. 9, no. 4, 1875-1890, 2018, doi: 10.11591/ijpeds.v9.i4.pp1875-1890.
[19] H. Chojaa, A. Derouich, M. Taoussi, O. Zamzoum, and M. Yessef, "Optimization of DFIG wind turbine power quality through adaptive fuzzy control," in *Digital Technologies and Applications, ICDTA 202. In Lecture Notes in Networks and Systems*, vol. 211, pp. 1235-1244, 2021, doi: 10.1007/978-3-030- 73882-2_113.
[20] M. Loucif, A. Boumediene, and A. Mechernene, "Maximum Power Point Tracking Based on Backstepping Control of Wind Turbine," in *Electrotehnica, Electronica, Automatica*, vol. 104, no. 62, pp. 103-108, 2014.
[21] R. Robinett III, D. Rush, and David G. Wilson, "Nonlinear Power Flow Control Design: Utilizing Exergy, Entropy, Static and Dynamic Stability, and Lyapunov Analysis," London: Springer-Verlag London, 2011.
[22] O. Zamzoum, Y. El Mourabit, M. Errouha, A. Derouich, and A. El Ghzizal, "Power control of variable speed wind turbine based on doubly fed induction generator using indirect field-oriented control with fuzzy logic controllers for performance optimization," in *Energy Sci Eng.*," vol. 6, no. 5, pp. 408-423, 2018, doi: https://doi.org/10.1002/ese3.215.
[23] M. Fdaili, A. Essadki, I. Kharchouf and T. Nasser, "An overall modeling of wind turbine systems based on DFIG using conventional sliding mode and second-order sliding mode controllers," *2019 International Conference on Wireless Technologies, Embedded and Intelligent Systems (WITS)*, 2019, pp. 1-6, doi: 10.1109/WITS.2019.8723837.
[24] C. Hamid, A. Derouich, M. Taoussi, O. Zamzoum and A. Hanafi, "An Improved Performance Variable Speed Wind Turbine Driving a Doubly Fed Induction Generator Using Sliding Mode Strategy," *2020 IEEE 2nd International Conference on Electronics, Control, Optimization and Computer Science (ICECOCS)*, 2020, pp. 1-8, doi: 10.1109/ICECOCS50124.2020.9314629.
[25] O. Zamzoum, Y. El Mourabit, M. Errouha, A. Derouich, A. Derouich, "Active and reactive power control of wind turbine based on doubly fed induction generator using adaptive sliding mode approach," in *Int. J. Adv. Comput. Sci. Appl.*, vol. 10, pp. 397-406, 2019, doi: 10.14569/IJACSA.2019.0100252.
[26] H. Buhler, Adjustment by slip mode (in French), Presses Polytechniques romandes, Lausanne, 1986.
[27] A. F. Zohra, B. I. Khalil, L. Slimane, S. Youcef, and M. Benyounes, "Artificial intelligence control applied in wind energy conversion system," in *International Journal of Power Electronics and Drive Systems*, vol. 9, no. 2, pp. 571-578, doi: 10.11591/ijpeds.v9.i2.pp571-578, 2018.
[28] I. Yasmine, E. B. Chakib, B. Badre, "Power control of DFIG-generators for wind turbines variable-speed," in *International Journal of Power Electronics and Drive Systems*," vol. 8, no. 1, pp. 444-453, 2017, doi: 10.11591/ijpeds.v8.i1.pp444-453.
[29] R. Chakib, A. Essadki, and M. Cherkaoui, "Modeling and control of a wind system based on a DFIG by active disturbance rejection control," in *International Review on Modeling and Simulations*, vol. 7, no. 4, pp. 626-637, 2014, 10.15866/iremos.v7i4.2386.
[30] M. Yessef, B. Bossoufi, M. Taoussi, A. Lagrioui, and H. Chojaa, "Improved Hybrid Control Strategy of the Doubly-Fed Induction Generator Under a Real Wind Profile, "*Digital Technologies and Applications. ICDTA 2021. Lecture Notes, in Networks and Systems*, vol 211, pp. 1279-1290, 2021, doi: 10.1007/978-3-030-73882-2_117 2_117.